chemosensors

MDPI

Communication

Quantitative Fiber-Enhanced Raman Sensing of Inorganic Nitrogen Species in Water

Hugo Kerdoncuff *, Lisa C. Deleebeeck and Mikael Lassen

Danish Fundamental Metrology, Kogle Allé 5, 2970 Hørsholm, Denmark; ldl@dfm.dk (L.C.D.); ml@dfm.dk (M.L.)
* Correspondence: hk@dfm.dk

Abstract: Fast and efficient water quality monitoring is essential in the pursuit of reducing the impact of human activities on the environment. We address this issue by presenting a sensing system and method based on Raman spectroscopy in liquid-filled capillaries, that enables quantitative measurement of polyatomic anions in solution. We demonstrate quantitative measurement of nitrate concentrations in water via multivariate analysis with partial least squares regression. We achieve a limit of detection of 0.13 millimolar for a measurement time of 30 s. Our Raman method is compared with gravimetrically measured concentration with good agreement and reproducibility. The Raman monitoring method can be performed in a continuous manner, thus suitable for fast continuous monitoring of water and wastewater quality.

Keywords: fiber-enhanced Raman spectroscopy; nitrate; quantitative analysis; water quality

check for updates

Citation: Kerdoncuff, H.; Deleebeeck, L.C.; Lassen, M. Quantitative Fiber-Enhanced Raman Sensing of Inorganic Nitrogen Species in Water. *Chemosensors* **2021**, *9*, 29. https://doi.org/10.3390/chemosensors9020029

Academic Editors: Marco Pisco and Rajapandiyan Panneerselvam
Received: 30 December 2020
Accepted: 27 January 2021
Published: 31 January 2021

Publisher's Note: MDPI stays neutral with regard to jurisdictional claims in published maps and institutional affiliations.

Copyright: © 2021 by the authors. Licensee MDPI, Basel, Switzerland. This article is an open access article distributed under the terms and conditions of the Creative Commons Attribution (CC BY) license (https://creativecommons.org/licenses/by/4.0/).

1. Introduction

The control and preservation of water quality is one of the major global environmental challenges as it concerns human populations due to increased scarcity of access to safe drinking water [1], and ecosystems via chemical contamination and eutrophication resulting from industrial and agricultural activities [2]. Among water pollutants, polyatomic ions such as nitrates, sulfates, nitrites, and phosphates are often the result of runoff from fertilizers and animal feedlots, and effluents from sewage treatment plants. They are very soluble in water and end up contaminating groundwater, rivers, and lakes. By accelerating the eutrophication in water ecosystems, this has a very negative impact on the environment and public health. Current standard measurement methods for ionic concentrations includes colorimetry, ion chromatography, capillary electrophoresis, ion selective electrodes, electrolytic conductivity [3], mass spectrometry, and UV spectrophotometry [4]. Each have their advantages and inconveniences in regards to sensitivity, accuracy, cost, and complexity, but often require sample preparation, use of reagent or frequent calibration, and/or are specific to one species only.

Raman spectroscopy is a well-known technique for chemical analysis of a wide variety of materials, gas, liquids, and solids [5–7]. It enables detection and quantification of multiple dissolved substances in water without the need of sample preparation or reagents, which makes it a powerful method for online and in situ measurements [8,9]. Quantitative measurements of ion concentrations in water can be realized by calibrating the Raman scattering intensity against reference concentrations [10–13]. Due to the distinct vibrational spectra of different molecular species, it is possible to measure the concentration of multiple species with a single measurement, thereby providing rich chemical information on a sample in a short time. However, a major drawback of Raman spectroscopy is that the spontaneous Raman scattering effect is very weak. Therefore, long acquisition times and high optical excitation powers are typically required to reach sufficient sensitivity for low concentration measurements [13,14]. However, different techniques for enhancing Raman scattering efficiency can be applied to circumvent these limitations, such as UV resonance Raman spectroscopy [15] and surface-enhanced Raman spectroscopy (SERS) [16,17].

In this work, we apply fiber-enhanced Raman spectroscopy (FERS) to increase the sensitivity of concentration measurements and lower requirements on optical power and measurement times. The FERS method relies on the confinement of both the excitation laser and the sample within the core of a light-guiding capillary, thereby increasing the interaction between light and analyte over the length of the capillary [18]. To date, selectively filled hollow-core photonic crystal fibers and antiresonant fibers are the most efficient capillaries for FERS, reaching sensitivities down to a few micromolar (μM) in concentration measurements [19,20]. Their higher numerical aperture compared to other liquid-filled capillaries enables better collection of the scattered light [21]. However, their availability is limited and they require delicate preparation steps with specialized equipment before use, which restricts their application to dedicated laboratories. On the other hand, capillary tubes made of a material with refractive index lower than that of water (i.e., n < 1.33), such as Teflon™AF 2400 (n = 1.29), are readily available from commercial suppliers and do not require any preparation beside cutting to the desired length. These are convenient to use and provide significant improvement over Raman measurements in cuvettes [21–23].

We present a method for quantitative measurements of nitrate concentration in water by FERS in a Teflon™AF 2400 capillary. We apply a multivariate analysis method with partial least squares regression (PLSR) and calculate standard uncertainty of concentration measurements of unknown samples, as well as limit of detection (LOD) and limit of quantitation (LOQ) of the measurement method. We demonstrate an LOD of 0.13 millimolar (mM) with a measurement time of 30 s, which is sufficient to detect nitrate thresholds of water drinkability recommended by the World Health Organization (<0.8 mM [24]). Our measurement method enables continuous and repeated measurements on flowing liquid samples without the use of any reagent and can be adapted to measurement of other molecules, making it suitable for on site continuous monitoring of multiple dissolved polyatomic substances in water.

2. Materials and Methods

2.1. Preparation of Solutions

Salts of sodium nitrate ($NaNO_3$) and potassium nitrate (KNO_3) were purchased from Sigma-Aldrich Co., with specified purity of 99.995% and 99.999%, respectively. Nitrate solutions with concentrations ranging from 0.1 mM to 100 mM were prepared gravimetrically by dilutions in ultrapure water (UPW) (Milli-Q®). The weights of each salt and UPW were measured on calibrated balances (Mettler Toledo). Molar concentrations are converted from mass fractions of solute in solution by using the molar masses of $NaNO_3$ ($M_{NaNO_3} = 84.9947(5)$ g/mol) and KNO_3 ($M_{KNO_3} = 101.1032(5)$ g/mol), and the density of the solutions ($\rho = 1.000(3)$ kg/L). The variability of environmental conditions during solution preparation were taken into account in the uncertainty assigned to the density of solution (including air buoyancy corrections). Uncertainties of the density of the solution and of the mass of solute are the main contributions to the standard uncertainty of the molar concentrations.

2.2. Experimental Setup and Operation

The experimental setup for FERS shown in Figure 1 is similar to the one presented by Frosch et al. in [23]. A syringe pump (KDS 100 Legacy Syringe Pump) controls the flowing of liquid sample through a Tygon® tubing with inner diameter ID = 508 μm (Elveflow), towards a custom-made adapter that connects to a capillary of Teflon™AF 2400 with inner diameter ID = 76 μm and outer diameter OD = 508 μm (Biogeneral Inc., San Diego, CA, USA). The adapter has three 10–32 coned ports for fastening tubing of outer diameter OD = 1/16 inches with nuts and ferrules. The capillary is fitted in the central port with a tubing sleeve (IDEX F-244 NanoTight™) made of undyed fluorinated ethylene propylene (FEP) to minimize fluorescence background.

An optical window (uncoated Infrasil® window, Thorlabs Inc., Newton, NJ, USA) in the adapter allows coupling of light in and out of the liquid-filled capillary. A microscope

objective with 10× magnification focuses the excitation laser light into the capillary and collects the backscattered Raman light. It offers sufficient working distance through the optical window and a numerical aperture NA = 0.25 that is near that of the liquid-filled capillary. We use laser excitation at a wavelength of 532 nm and filter it from the collected Stokes backscattered light with a longpass dichroic mirror (Semrock Inc., New York city, NY, USA). The Stokes light is then directed to a spectrometer (iHR320, Horiba Jobin Yvon) equipped with a thermoelectrically cooled CCD detector (Synapse CCD, Horiba Jobin Yvon). All measurements were performed with a slit size of 200 µm and a static holographic diffraction grating with 1800 gr/mm.

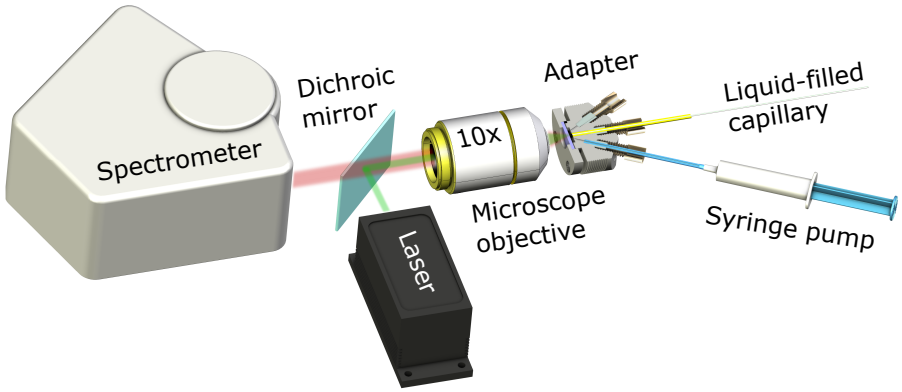


Figure 1. Experimental setup of our fiber-enhanced Raman spectroscopy (FERS) method. The liquid sample is pushed by a syringe pump towards a custom-made adapter that connects to the capillary of Teflon™AF 2400. Once filled with the liquid sample, the capillary guides light by total internal reflection thereby enhancing interaction between light and sample. The 10× microscope objective focuses the excitation laser light at 532 nm through a transparent window on the adapter and into the capillary, and collects the Raman backscattered light from the capillary. The dichroic mirror separates the excitation laser light and the Stokes backscattered light that is directed to the Horiba spectrometer.

Samples were steadily flowed through the capillary during measurements. The sample path was rinsed with UPW between each measurement. The rinsing procedure was validated during preliminary tests of the setup by confirming the absence of any detectable signal from NO_3^- from a UPW sample after rinsing. At present, manual operations are required to switch between samples during calibration and measurements. However, it is possible to implement automated operation as a future improvement of the system by using a commercially-available sequential fluid injection systems.

The adapter is designed with an SM1 external threading for mounting on standard optical mounts. In addition to the custom-made adapter part, all parts of the setup are commercially available and can be conveniently integrated to common Raman microscopes and setups at a relatively low cost.

2.3. Calculation of Standard Uncertainty, LOD, and LOQ for Multivariate PLSR

The standard uncertainty of the measurement of an unknown sample concentration for a multivariate PLSR is calculated from the variance of the predicted unknown concentration $\hat{y}_u$, given by [25,26]

$$\sigma^2_{\hat{y}_u} = \left(N^{-1} + h_u\right)\sigma^2_{\Delta y} + \left(N^{-1} + h_u\right)\|\mathbf{B}\|^2\sigma^2_{\Delta X} + \|\mathbf{B}\|^2\sigma^2_{\Delta X}, \quad (1)$$

where $\sigma^2_{\Delta y}$ and $\sigma^2_{\Delta X}$ are the variances of the calibration concentration and spectra errors, respectively, N is the number of calibration samples, h_u is the leverage of the unknown sample, and $\|\mathbf{B}\|$ is the norm of the regression coefficient of the calibration model. The first term on the right-hand side represents a contribution from the calibration concentration error. The second and third terms represent contributions from errors of the calibration

and unknown sample spectra, respectively. Due to near identical measurement conditions for calibration and unknown samples, the variance of the spectra error $\sigma^2_{\Delta X}$ is considered equal for all samples. The leverage h_u is a dimensionless factor that places the sample relative to the calibration space. It is calculated from the generalized inverse of the score matrix of the calibration samples $\mathbf{T}^+$ and the score vector of the unknown sample $\mathbf{T}_u$ as $h_u = \|\mathbf{T}_u^T \mathbf{T}^+\|^2$ [26]. The N^{-1} factor in Equation (1) accounts for the mean centering of the data by the PLSR algorithm.

The LOD corresponds to the minimum analyte concentration that can be distinguished from the absence of the analyte (i.e., blank sample) and the LOQ corresponds to the analyte concentration for which the prediction uncertainty is at most 10% of the predicted concentration. The LOD and LOQ for multivariate analysis are defined by [26]

$$LOD = 3.3\sigma_{\hat{y}_0}, \quad LOQ = 10\sigma_{\hat{y}_0}, \tag{2}$$

where $\sigma^2_{\hat{y}_0}$ is the variance of the predicted concentration of a blank sample (i.e., UPW) and follows the definition of Equation (1).

3. Results

3.1. Setup Characterization

The measurement parameters for acquisition of Raman spectra for calibration and quantitative analysis of nitrate solutions were determined by preliminary characterization and testing of the setup. For this purpose, we estimated the signal-to-noise ratio (SNR) of the intensity of the Raman peak of nitrate ions (NO_3^-) at 1047 cm^{-1}. The intensity of the Raman peak was extracted from a fit to the Raman spectrum measured between 921 cm^{-1} and 1950 cm^{-1} (see Figure 2a). Raman peaks of NO_3^- at 1047 cm^{-1} and water at 1637 cm^{-1} (H-O-H bending mode) were fitted with pseudo-Voigt profiles and the baseline by a fourth degree polynomial. The noise was calculated as the standard deviation of the spectral noise in the range 950 cm^{-1} to 1000 cm^{-1} after removing the baseline. Figure 2b shows the Raman peak of NO_3^- with pseudo-Voigt fit after baseline removal using 0.85 mW optical power for excitation and illustrates our definition of signal and noise. From the SNR, we derive the limit of detection (LOD) of NO_3^- in solution as a more meaningful figure of merit, SNR_{LOD} = 3.3 (Equation (2)).

We estimated the LOD as a function of laser excitation power at the sample and observed a behavior proportional to the inverse square root of the optical power, as expected from Poissonian light statistics. Figure 2c shows signal, noise, and calculated LOD for measurements of 11.74(5) mM of $NaNO_3$ as a function of optical power at the sample. Mean values and standard deviations are estimated from three measurements for each power level. Measurements are realized with a capillary length of 104 mm and consists of the average of ten acquisitions of one second each. Signal and noise were fitted with linear and square root functions, respectively, and estimates of the LOD are calculated from these fits.

The effect of capillary length on the signal enhancement was assessed by a cutback measurement, where the intensity of the Raman signal was measured as a function of capillary length [22]. We measured an attenuation length of 13 cm (attenuation coefficient of 0.34 dB/cm), which is about one order of magnitude lower than previously reported values for Teflon™AF 2400 capillaries filled with water [21]. The lower performance of our filled capillaries might be due to imperfection in the capillaries due to the manufacturing process. Capillaries with larger core diameters may also provide better light-guiding properties [22].

Following the initial investigative measurements, the following measurement parameters for calibration and quantitative analysis were chosen: 20 acquisitions of 1.5 s with an optical power of 40 mW at the sample and a capillary length of 89 mm. This provides an LOD of NO_3^- below the water drinkability limit of 0.8 mM with a total acquisition time per spectrum of 30 s in order to provide fast measurements that remain comparable to sensing techniques with similar sensitivity [4]. Optical power of the excitation laser and

acquisition time were balanced to fill the full well capacity of the CCD detector while preventing saturation.

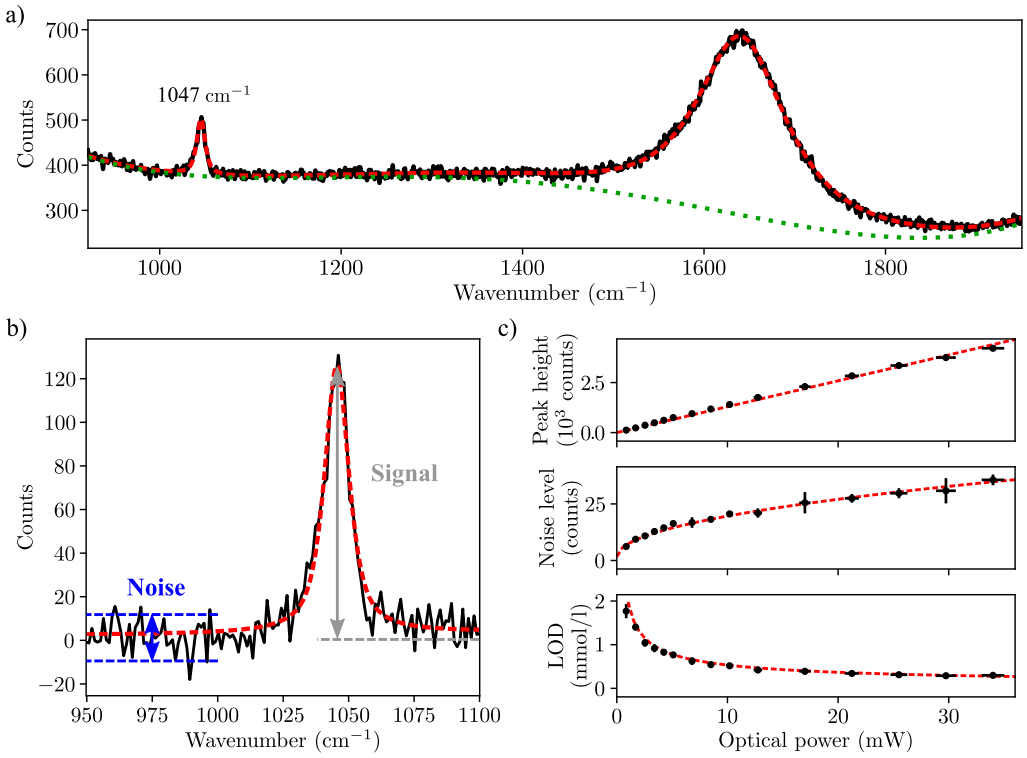


Figure 2. (**a**) Raman spectrum of a solution of 11.74(5) mM of $NaNO_3^-$ (black line) with fit (red dashed line) and polynomial baseline (green doted line). Raman peaks of NO_3^- at 1047 cm^{-1} and water at 1637 cm^{-1} (H-O-H bending mode) are fitted with pseudo-Voigt profiles. A zoom in on the Raman peak of NO_3^- after baseline removal is shown in (**b**) with pseudo-Voigt fit (red dashed line). Blue and gray arrowed lines illustrate noise and signal amplitudes, respectively. Optical power at the sample was set at 0.85 mW. (**c**) Signal, noise, and calculated LOD for measurements of 11.74(5) mM of $NaNO_3$ as a function of optical power at the sample. Vertical error bars represent standard deviations estimated from three measurements for each power level. Horizontal error bars correspond to ±3% uncertainty of the power meter reading according to specifications.

3.2. Calibration Model

To demonstrate the performance of our quantitative measurement method for nitrate concentrations, we realized a calibration curve on a series of known concentrations of $NaNO_3$ and predicted the concentrations of NO_3^- in solutions of $NaNO_3$ and KNO_3. The calibration curve correlates the instrument response, i.e., Raman spectra, to the concentrations of the analyte. It is built upon a set of known concentrations and their measured Raman spectra and enables subsequent predictions of unknown sample concentrations from their measured Raman spectra [26]. Our calibration curve is based on measurements of 10 solutions with concentrations 0 mM (UPW), 0.118(1) mM, 0.236(1) mM, 0.353(2) mM, 0.589(3) mM, 0.941(4) mM, 1.177(5) mM, 1.411(7) mM, and 2.355(10) mM. Each solution was measured three times providing a set of 30 calibration points. Raman spectra were acquired in the range 921 cm^{-1} and 1950 cm^{-1} without moving the diffraction grating of the spectrometer for best wavenumber precision and repeatability. The calibration curve was made by PLSR in order to separate the influence of nitrate concentration on peak height from slight modification of the baseline due to small changes in alignment and guiding of laser light after rinsing and replacing samples. The number of components and the postprocessing operations of the data were determined by validating the model on a set of 45 spectra of known solutions of of known concentrations of $NaNO_3$ and KNO_3. We

optimized our calibration model by minimizing the root-mean-squared error of prediction (RMSEP) and maximizing the regression coefficient (R^2) of the validation set, defined by

$$RMSEP = \left[\frac{1}{n}\sum_{i=1}^{n}(y_i - \hat{y}_i)^2\right]^{\frac{1}{2}}, \quad R^2 = 1 - \frac{\sum_{i=1}^{n}(y_i - \bar{y})^2}{\sum_{i=1}^{n}(y_i - \hat{y}_i)^2} \tag{3}$$

where n is the number of samples in the data set, y_i are the known concentration values, $\bar{y}$ their mean, and $\hat{y}_i$ are the predicted concentration values. The resulting model uses two components and involves postprocessing of the spectra by normalization to the Raman peak of the solvent water at 1637 cm^{-1} and selection of spectral data in the range 1000 cm^{-1} to 1090 cm^{-1} (Figure 3a). The Raman peak of water is used as an internal reference to correct for fluctuations in laser intensity, coupling efficiency to the light-guiding capillary, and collection efficiency of the backscattered light [13,20,23,27]. Our calibration model achieves $RMSEP_{cal}$ = 0.05 mM and R^2_{cal} = 0.996 on the calibration set, and $RMSEP_{val}$ = 0.07 mM and R^2_{val} = 0.989 on the validation set. The validation spectra were acquired with similar measurement settings during a preliminary development phase of the setup and display a higher variability of the shape of the baseline compared to the calibration set. This explains the higher RMSEP and lower R^2 values obtained on the validation set but shows that our calibration model takes into account differences in the shape of spectra that are due to measurement conditions. Figure 3b shows the predicted concentrations of the calibration set using our PLSR model.

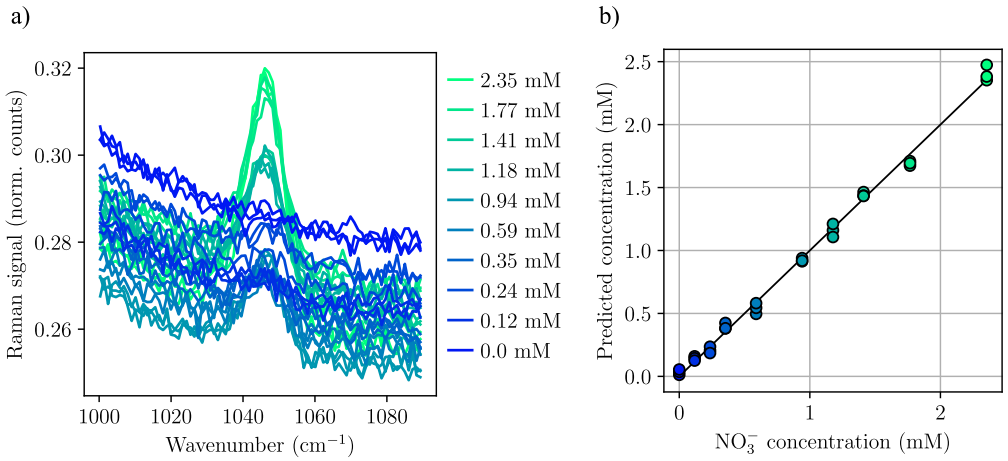


Figure 3. (**a**) Spectral data of the calibration set obtained by measurement of 10 solutions of $NaNO_3$ and normalization to the Raman peak of the solvent water at 1637 cm^{-1}. Differences in baseline are mainly due to small changes in alignment and guiding of laser light after rinsing and replacing samples in the capillary. (**b**) Predicted NO_3^- concentrations of the 30 spectra of the calibration set using our PLSR model.

3.3. Measurement of Unknown Concentrations

To evaluate the validity of our method, we predicted the concentrations of four a priori unknown samples. Two solutions of $NaNO_3$ and two solutions of KNO_3 were prepared and measured with our method. The results were a posteriori compared with the concentration values obtained by gravimetric measurement during preparation. The comparison of measured values and their standard uncertainties are shown in Table 1, where the standard uncertainties are the square root of the variances given by Equation (1).

Our results demonstrate good accuracy of the predicted concentration down to the LOQ. Using Equation (2), we calculate LOD = 0.13 mM and LOQ = 0.40 mM from measurement of a blank sample with the FERS method.

Table 1. Comparison of gravimetrically measured concentrations and predicted concentrations with our FERS method.

Solution	Gravimetric (mM)	FERS (mM)
$NaNO_3$	0.391(2)	0.40(4)
$NaNO_3$	0.668(3)	0.68(4)
KNO_3	0.394(2)	0.42(4)
KNO_3	0.668(3)	0.62(4)

4. Discussion

We presented a quantitative method for sensing of NO_3^- in aqueous solutions by applying the FERS measurement technique with a multivariate PLSR analysis method. Our method enables measurement of NO_3^- concentration in 30 s with a LOD of 0.13 mM and LOQ of 0.40 mM, which provides an improvement over one order of magnitude compared to standard Raman spectroscopy method in cuvettes [13]. The FERS setup can be conveniently implemented in analysis laboratory already equipped with Raman instrumentation as it uses low-cost and commercially available components, except for a custom-made adapter of simple design [23].

We applied our method to measure nitrate anion concentrations in the presence of two different cations (Na^+ and K^+) and showed a good accuracy of the predicted concentrations. However, we observe a slightly larger discrepancy between known and predicted concentrations in KNO_3 solutions (see Table 1) which might be due to our use of $NaNO_3$ solutions only for calibration. Nevertheless, we do not expect the cation to have a significant influence on the Raman spectrum of the anion and of the H-O-H bending mode of the solvent water at millimolar concentration levels and below and at our level of sensitivity [13,28]. At higher concentrations on the order of 100 mM, weaker Raman bands of the ions may rise significantly above noise levels and affect the calibration method [13]. In our work, we focused on measuring concentrations below 1 mM and have not determined the high concentration limit of our method. Further investigation is required to analyze influences of different salt solutions and correct other potential source of variability in the measurement, as explained below.

The main source of instability and inaccuracy of our measurement system comes from the process of rinsing and replacing samples in the capillary. The effect is a slight modification of the shape of the baseline that introduces more variability in the spectral data. We attribute these modifications to small movements of the capillary that changes the alignment with the focused laser beam. Our calibration method applying PLSR with two components is capable of removing such effects to some extent. It can be further improved by imposing tighter tolerances on the machining of the custom-made adapter. Moreover, the manual operation of replacing samples may introduce air bubbles in the system. This can be prevented by the implementation of a sequential fluid injection system for sample loading, which further brings the possibility of automatizing the calibration and measurement procedure.

Our system can be adapted to analysis of wastewater by filtering the sample in order to remove particles that compromise light guiding in the capillary. Filtration has been commonly applied for analysis of soluble components in murky water samples [15,17]. Compared to previously reported nitrate detection methods in wastewater using spontaneous Raman spectroscopy [10,11], our solution enables a significant reduction of measurement time and optical power requirements without increasing the complexity of the measuring system and its operation. The FERS method also has the advantage of providing a homogeneous enhancement of the collected Raman scattering intensity from all constituents of the sample, such that it preserves the selectivity of spontaneous Raman scattering methods. The enhancement is dependent on the transmission spectrum of the liquid-filled capillary. In contrast, the SERS method is highly susceptible to interference from other species due to the surface chemistry of the SERS substrates [16,17]. Moreover,

it requires a sample preparation step and the use of consumables, as the SERS substrates cannot be reused for subsequent measurements and needs to be replaced. Therefore, SERS is not suited for continuous autonomous measurement. UV resonance Raman spectroscopy is a powerful method for low concentration measurements of nitrates and nitrites at micromolar levels [15]; however, it requires bulky gas lasers and specific UV optics. The signal enhancement by resonance Raman scattering is dependent on the energy of electronic transitions of the molecules so that not every species in a sample is affected. This limits the variety of analytes that can be probed by the technique. Nevertheless, the FERS method can be combined with UV resonance Raman scattering to further improve the sensitivity of concentration measurements [23].

We firmly believe that our FERS method with multivariate PLSR can be applied to simultaneous quantitative measurements of concentrations of polyatomic ions in aqueous solutions due to the specificity of the Raman spectra of different molecular species. For example, nitrates, nitrites, phosphates, and sulfates have distinguishable Raman bands in the region around 1000 cm^{-1} [13]. Furthermore, multivariate analysis is able to separate contributions of even overlapping components in spectral data [29]. Therefore, our method is promising for continuous monitoring of water quality. The sensitivity of the method can also be improved significantly in combination with UV resonance Raman spectroscopy that can bring the LOD down to the micromolar level [15,23]. This will be the focus of future work.

Author Contributions: Conceptualization, H.K.; methodology, H.K.; software, H.K.; validation, H.K.; formal analysis, H.K.; investigation, H.K.; resources, H.K., M.L. and L.C.D.; data curation, H.K.; writing—original draft preparation, H.K.; writing—review and editing, H.K., M.L., and L.C.D.; visualization, H.K.; supervision, H.K. and M.L.; project administration, H.K. and M.L.; funding acquisition, H.K. and M.L. All authors have read and agreed to the published version of the manuscript.

Funding: This research was funded by the Danish Agency for Institutions and Educational Grants and the Innovation Fund Denmark (IFD) under Eurostars project Bacsens (case No. 9046-00032A).

Institutional Review Board Statement: Not applicable.

Informed Consent Statement: Not applicable.

Data Availability Statement: Data sharing not applicable.

Acknowledgments: The authors thank Alan Snedden for his help in calculating standard uncertainties of gravimetrically measured concentrations.

Conflicts of Interest: The authors declare no conflict of interest. The funders had no role in the design of the study; in the collection, analyses, or interpretation of data; in the writing of the manuscript, or in the decision to publish the results.

References

1. World Health Organization. *Progress on Household Drinking Water, Sanitation and Hygiene 2000–2017*; United Nations Children's Fund (UNICEF): New York, NY, USA; World Health Organization: Geneva, Switzerland, 2019.
2. Peters, N.E.; Meybeck, M.; Chapman, D.V. Effects of human activities on water quality. In *Encyclopedia of Hydrological Sciences*; Anderson, M.G., McDonnell, J.J., Eds.; John Wiley and Sons: Hoboken, NJ, USA, 2005.
3. Thirstrup, C.; Deleebeeck, L.C. Review of electrolytic conductivity sensors. *IEEE Trans. Instrum. Meas.* **2020**, under review.
4. Rice, E.W.; Baird, R.B.; Eaton, A.D. (Eds.) Inorganic nonmetallic constituents. In *Standard Methods for the Examination of Water and Wastewater*; Part 4000; American Public Health Association: Washington, DC, USA; American Water Works Association: Washington, DC, USA; Water Environment Federation: Washington, DC, USA, 2017.
5. Lewis, I.R.; Edwards, H.G.M. (Eds.) *Handbook of Raman Spectroscopy: From the Research Laboratory to the Process Line*; Marcel Dekker: New York, NY, USA, 2017.
6. Das, R.S.; Agrawal, Y.K. Raman spectroscopy: Recent advancements, techniques and applications. *Vib. Spectrosc.* **2011**, *57*, 163–176. [CrossRef]
7. Nakamoto, N. *Infrared and Raman Spectra of Inorganic and Coordination Compounds*; John Wiley and Sons: Hoboken, NJ, USA, 2009.
8. Brewer, P.G.; Malby, G.; Pasteris, J.D.; White, S.N.; Peltzer, E.T.; Wopenka, B.; Freeman, J.; Brown, M.O. Development of a laser Raman spectrometer for deep-ocean science. *Deep Sea Res. Part I Oceanogr. Res. Pap.* **2004**, *51*, 739–753. [CrossRef]

9. Li, L.; Zhang, X.; Luan, Z.; Du, Z.; Xi, S.; Wang, B.; Cao, L.; Lian, C.; Yan, J. In situ Raman quantitative detection of methane concentrations in deep-sea high-temperature hydrothermal vent fluids. *J. Raman Spectrosc.* **2020**, *51*, 2328–2337. [CrossRef]
10. Furuya, N.; Matsuyuki, A.; Higuchi, S. Determination of nitrate ion in waste and treated waters by laser Raman spectrometry. *Water Res.* **1979**, *13*, 371–374. [CrossRef]
11. Lombardi, D.R.; Wang, C.; Sun, B.; Fountain, A.W.; Vickers, T.J.; Mann, C.K.; Reich, F.R.; Douglas, J.G.; Crawford, B.A.; Kohlasch, F.L. Quantitative and Qualitative Analysis of Some Inorganic Compounds by Raman Spectroscopy. *Appl. Spectrosc.* **1994**, *48*, 875–883. [CrossRef]
12. Murata, K.; Kawakami, K.; Matsunaga, Y.; Yamashita, S. Determination of sulfate in brackish waters by laser Raman spectroscopy. *Anal. Chim. Acta* **1997**, *344*, 153–157. [CrossRef]
13. Fontana, M.D.; Ben Mabrouk, K.; Kauffmann, T.H. Raman spectroscopic sensors for inorganic salts. *Spectrosc. Prop. Inorg. Organomet. Compd.* **2013**, *44*, 40–67.
14. Cunningham, K.M.; Goldberg, M.C.; Weiner, E.R. Investigation of Detection Limits for Solutes in Water Measured by Laser Raman Spectrometry. *Anal. Chem.* **1977**, *49*, 70–75. [CrossRef]
15. Ianoul, A.; Coleman, T.; Asher, S.A. UV Resonance Raman Spectroscopic Detection of Nitrate and Nitrite in Wastewater Treatment Processes. *Anal. Chem.* **2002**, *74*, 1458–1461. [CrossRef]
16. Mosier-Boss, P.A.; Lieberman, S.H. Detection of nitrate and sulfate anions by normal Raman spectroscopy and SERS of cationic-coated, silver substrates. *Anal. Chem.* **2000**, *54*, 1126–1135. [CrossRef]
17. Gajaraj, S.; Fan, C.; Lin, M.; Hu, Z. Quantitative detection of nitrate in water and wastewater by surface-enhanced Raman spectroscopy. *Anal. Chem.* **2013**, *185*, 5673–5681. [CrossRef] [PubMed]
18. Walrafen, G.E.; Stone, J. Intensification of Spontaneous Raman Spectra By Use of Liquid Core Optical Fibers. *Appl. Spectrosc.* **1972**, *26*, 585–589. [CrossRef]
19. Yan, D.; Popp, J.; Pletz, M.W.; Frosch, T. Highly Sensitive Broadband Raman Sensing of Antibiotics in Step-Index Hollow-Core Photonic Crystal Fibers. *ACS Photonics* **2017**, *4*, 138–145. [CrossRef]
20. Yan, D.; Frosch, T.; Kobelke, J.; Bierlich, J.; Popp, J.; Plets, M.W.; Frosch, T. Fiber-Enhanced Raman Sensing of Cefuroxime in Human Urine. *Anal. Chem.* **2018**, *90*, 13243–13248. [CrossRef] [PubMed]
21. Eftekhari, F.; Irizar, J.; Hulbert, L.; Helmy, A.S. A comparative study of Raman enhancement in capillaries. *J. Appl. Phys.* **2011**, *109*, 113104. [CrossRef]
22. Altkorn, R.; Koev, I.; Pelletier, M.J. Raman Performance Characteristics of Teflon™-AF 2400 Liquid-Core Optical-Fiber Sample Cells. *Appl. Spectrosc.* **1999**, *53*, 1169–1176. [CrossRef]
23. Frosch, T.; Yan, D.; Popp, J. Ultrasensitive Fiber Enhanced UV Resonance Raman Sensing of Drugs. *Anal. Chem.* **2013**, *85*, 6264–6271. [CrossRef]
24. Edition, F. *Guidelines for Drinking-Water Quality: Fourth Edition Incorporating the First Addendum*; World Health Organization: Geneva, Switzerland, 2017.
25. Faber, K.; Kowalski, B. Propagation of measurement errors for the validation of predictions obtained by principal component regression and partial least squares. *J. Chemom.* **1997**, *11*, 181–238. [CrossRef]
26. Olivieri, A.C. Analytical Figures of Merit. In *Introduction to Multivariate Calibration: A Practical Approach*; Springer International Publishing: Cham, Switzerland, 2018; pp. 159–177.
27. Duraipandian, S.; Knopp, M.M.; Pollard, M.R.; Kerdoncuff, H.; Petersen, J.C.; Müllertz, A. A fast and novel internal calibration method for quantitative Raman measurements on aqueous solutions. *Anal. Methods* **2018**, *10*, 3589–3593. [CrossRef]
28. Ben Mabrouk, K.; Kauffmann, T.H.; Aroui, H.; Fontana, M.D. Raman study of cation effect on sulfate vibration modes in solid state and in aqueous solutions. *J. Raman Spectrosc.* **2013**, *44*, 1603–1608. [CrossRef]
29. Duraipandian, S.; Petersen, J.C.; Lassen, M. Authenticity and concentration analysis of extra virgin olive oil using spontaneous Raman spectroscopy and multivariate data analysis. *Appl. Sci.* **2019**, *9*, 2433. [CrossRef]